Journal of Magnetics 7(3), 80-93 (2002)

Exchange Anisotropy of Polycrystalline Ferromagnetic/ Antiferromagnetic Bilayers

Masakiyo Tsunoda* and Migaku Takahashi

Department of Electronic Engineering, Tohoku University, Aobayama 05, Sendai 980-8579, Japan

(Received 2 August 2002)

The role of magnetic anisotropy of the antiferromagnetic layer on the magnetization process of exchange coupled polycrystalline ferromagnetic/antiferromagnetic bilayers is discussed. In order to elucidate the magnetic torque response of Ni-Fe/Mn-Ir bilayers, the single spin ensemble model is newly introduced, taking into account the two-dimensionally random distribution of the magnetic anisotropy axes of the antiferromagnetic grains. The mechanism of the reversible inducement of the exchange anisotropy along desirable directions by field cooling procedure is successfully explained with the new model. Unidirectional anisotropy constant, J_K, of polycrystalline Ni-Fe/Mn-Ir and Co-Fe/Mn-Ir bilayers is investigated as functions of the chemical composition of both the ferromagnetic layer and the antiferromagnetic layer. The effects of microstructure and surface modification of the antiferromagnetic layer on J_K are also discussed. As a notable result, an extra large value of J_K, which exceeds 0.5 erg/cm^2, is obtained for $Co_{70}Fe_{30}/Mn_{75}Ir_{25}$ bilayer with the ultra-thin (50 Å~100 Å) Mn-Ir layer. The exchange anisotropy of $Co_{70}Fe_{30}$ 40 Å/$Mn_{75}Ir_{25}$ 100 Å bilayer is stable for thermal annealing up to 400 °C, which is sufficiently high for the application of spin valve magnetoresistive devices.

Key words : exchange anisotropy, exchange bias, magnetic anisotropy, multilayer, spin valve

1. Introduction

Exchange anisotropy, or exchange bias phenomenon, in bilayer of a ferromagnet (F) and an antiferromagnet (AF) has attracted a great deal of attentions in recent years due to its underlying physics and a central role in spin valve magnetoresistive devices used in magnetic random access memories or in read head technology for high-density recording systems [1]. However, a satisfactory understanding of this phenomenon and a general guiding principle to enlarge the biasing field have not been developed.

One of the important questions concerning the mechanism of the exchange anisotropy is the magnetic anisotropy of the AF layer. The original theoretical model for the exchange anisotropy, established by Meiklejohn and Bean (MB) [2, 3], assumes a coherent motion of AF spins throughout the reversal of the F layer magnetization and predicts that the exchange anisotropy is observed only when the AF moments are adhered to their magnetic anisotropy axes. The AF domain wall model that appeared next [4-6] also needs the magnetic anisotropy of the AF layer to form the twisted AF spin structures when the F layer magnetization reverses, adhering the AF moments at a distance from the interface by the magnetic anisotropy of the AF layer. In both the MB model and the domain wall model, a hysteresis loop of the F/AF bilayer is biased along the axis of the magnetic anisotropy of the AF layer, which is unified in the whole film plane. In these ways, the magnetic anisotropy of the AF layer is an indispensable factor for the physical understandings of the exchange bias phenomenon. Even on the industrial application of F/AF bilayers, one can not neglect the role of the magnetic anisotropy of the AF layer. A specific feature of polycrystalline F/AF bilayers, reversible inducement of exchange bias field in the F layer along any desirable directions by field cooling procedure, is utilized to align the magnetization direction of two F layers transverse to each other under a zero field in spin valve heads. If the mechanism of this well-known experimental fact is to be explained with using the above models, a reversible rotation of the magnetic anisotropy axis of the AF layer will be necessary. However, we do not deem it acceptable to assume the presence of reversible changes of the unified magnetic anisotropy of the AF layer by field cooling. Such the assumption seems to lack an attention

*Corresponding author: Tel: +81-22-217-7133, Fax: +81-22-263-9416, e-mail: tsunoda@ecei.tohoku.ac.jp

to the physical origin of the magnetic anisotropy of the AF layer.

From the application point of view, another important factor of the exchange anisotropy for spin valve magnetoresistance devices is to enlarge the biasing field of the pinned layers. The synthetic ferrimagnetic (Sy-ferri) structure has been proposed for pinned layers in order to satisfy this requirement apparently [7, 8]. Exchange anisotropy of F/AF bilayers is, however, essentially important even in the case of using Sy-ferri structure, because the direction of magnetization in one of the F layer in the Sy-ferri pinned layer should be fixed enough with AF layer against the external applied field. In particular for read head technology, it is also required to reduce the total thickness of spin valves, in order to achieve high recording density.

One of the objectives of this article is to provide a comprehensive understandings about the origin and the role of magnetic anisotropy of the AF layer in exchange coupled polycrystalline F/AF bilayers, by reviewing our own experimental and theoretical works, closely related to this matter. A major analytical tool for these works is classical magnetic torquemetry, one of the most powerful methods to investigate the magnetic anisotropy. In this article, we first describe in detail the magnetic torque response of polycrystalline Ni-Fe/Mn-Ir bilayers as a function of the AF layer thickness and the external applied field in section 3. In section 4, the experimental results are compared with computations based on the single spin ensemble model, which is established by the present authors as an expanded MB model for the polycrystalline bilayer systems. The single spin ensemble model is then examined to elucidate the experimental fact concerning the reversible inducement of the exchange anisotropy, mentioned above.

The other objective of this article is to provide a guideline for the experimental efforts to enlarge the strength of the exchange anisotropy for industrial applications. In section 5, we review our experimental works, concerning with the Co-Fe (or Ni-Fe)/Mn-Ir polycrystalline bilayers, which is a favorable system to achieve relatively strong exchange anisotropy with an ultra-thin AF layer.

2. Experimental Procedure

The specimens were fabricated on silicon wafers with a thermally oxidized layer, using a rf magnetron sputtering machine under the ultra clean sputtering process conditions described in Refs. 9-10 to enhance the structural homogeneity. Substrates were held at room temperature for the deposition. A magnetic field of 30 Oe was applied parallel to the films plane during the deposition of both the ferromagnetic layer and the Mn-Ir layer. The $Ni_{79}Fe_{21}$ /$Mn_{74}Ir_{26}$ films consisted of four layers, sub/Ta 50 Å/Ni-Fe 50 Å/Mn-Ir d_{AF}/Ta 50 Å. The thicknesses of the Mn-Ir layer, denoted by d_{AF}, ranged from 20 Å to 200 Å. There was no post deposition heat treatment or other processing for Ni-Fe/Mn-Ir bilayers, except for the cases particularly noticed. The Mn-Ir/Co-Fe system was investigated in the so-called 'bottom type' structure, in the formed sub/Ta 50 Å/Ni-Fe 20 Å/Cu 50 Å/$Mn_{100-x}Ir_x$ d_{AF}/$Co_{100-y}Fe_y$ 40 Å/Cu 10 Å/Ta 20 Å. The Ta/Ni-Fe/Cu trilayer, placed under the Mn-Ir layer, was used as an underlayer, which improves f.c.c.-(111) sheet texture of the specimens and enhances the exchange biasing field of the bilayers [11]. The Mn-Ir /Co-Fe specimens were normally annealed at 300 °C for 30 min in a magnetic field of 1 kOe along the same direction of the field applied during the deposition.

All measurements, except for the temperature dependence, were performed at room temperature. The film microstructure was examined by X-ray diffraction (XRD) and by transmission electron microscopy (TEM). Magnetization curves and hysteresis loops were measured by vibrating sample magnetometer (VSM) techniques above room temperature (RT) and superconducting quantum interference device (SQUID) magnetometer below RT. Determinations of the magnetic anisotropy and the rotational hysteresis loss were made from measurements of torque as a function of the in-plane field angle θ for fixed applied fields from 0 to 15 kOe. These data were obtained with a standard null method torque magnetometer with a sensitivity of about 1×10^{-3} dyn-cm.

Figure 1 shows a representative hysteresis loop of the net film magnetic moment m vs. the bipolar applied field H for a polycrystalline Ni-Fe/Mn-Ir bilayer. The magnetic

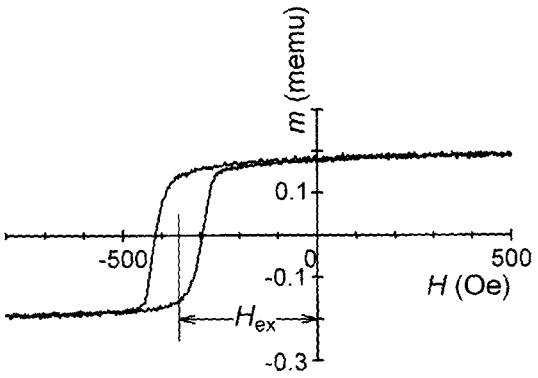

Fig. 1. A typical measured bilayer magnetization curve of the magnetic moment m versus the in plane magnetic field H. These specific data are for a polycrystalline Ni-Fe 50 Å/ $Mn_{74}Ir_{26}$ 50 Å bilayer. The shift of the loop is indicated by the exchange anisotropy field H_{ex}.

field was applied along the unidirectional axis defined by the deposition field. The data in Fig. 1 demonstrate the displaced loop character produced by the unidirectional exchange anisotropy as well as the usual hysteresis. The exchange bias field H_{ex} indicated in the figure provides a quantitative measure of the exchange anisotropy.

3. Magnetic torque analysis of polycrystalline Ni-Fe/Mn-Ir bilayers

3.1. Film microstructure

Figure 2 shows (a) measured and (b) calculated X ray diffraction profiles for a series of Ni-Fe/Mn-Ir bilayers with different AF layer thickness d_{AF} values. The calculations were done through the use of a step model [12, 13]. For these calculations, the film was taken to consist of a substrate with a 50 Å β-Ta layer, a 50 Å fcc Ni-Fe layer, an fcc $Mn_{75}Ir_{25}$ layer of thickness d_{AF} as indicated, and a final 50 Å thick β-Ta capping layer. The Ni-Fe and Mn-Ir layers were taken to be disordered. The lattice relationship between the substrate surface and the respective layers was taken to be substrate surface//Ta (002)// Ni-Fe (111)//Mn-Ir (111). The lattice spacings used for the calculations were 2.658 Å for the tantalum, 2.055 Å for the Ni-Fe, and 2.188 Å for the Mn-Ir. One can see good agreement between the measured and the calculated profiles. This agreement indicated that the films consist of highly coherent crystal planes which are stacked parallel to the film plane and that the thickness of the AF Mn-Ir layer in each case is uniform and accurate [14]. Figure 3 shows a TEM plan view and an electron diffraction pattern for the 200 Å thick Mn-Ir film fabricated with same film constitution of the bilayer, except for the capping Ta layer. This figure reveals Mn-Ir grains 100~200 Å in diameter. They have no preferred orientation in the film plane (the sheet texture is random in two dimensions) [15].

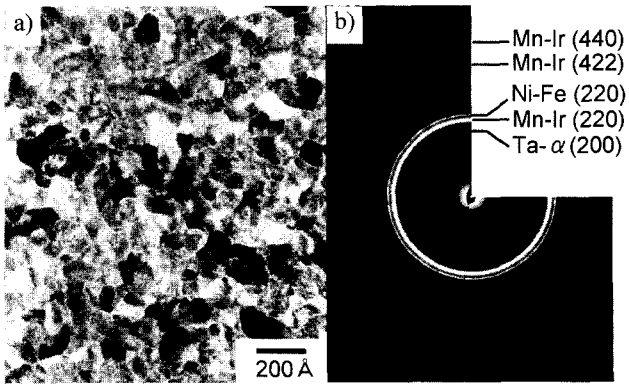

Fig. 3. (a) TEM plane view and (b) electron diffraction pattern of a 200 Å thick $Mn_{74}Ir_{26}$ film fabricated on a Ta 50 Å/Ni-Fe 50 Å underlayer. Ni-Fe and Mn-Ir (111) planes are oriented highly parallel to the film plane. The incident electron beam is perpendicular to the (111) plane of the Mn-Ir film.

3.2. Exchange bias field and magnetic torque response

Figure 4 shows the variation in the measured exchange bias field H_{ex} with the antiferromagnetic layer thickness [14]. These data show that H_{ex} becomes nonzero when d_{AF} exceeds about 25 Å, rises rapidly, reaches a peak value of about 370 Oe at d_{AF} ~75 Å, and then gradually decreases. If the peak in H_{ex} at 370 Oe is combined with

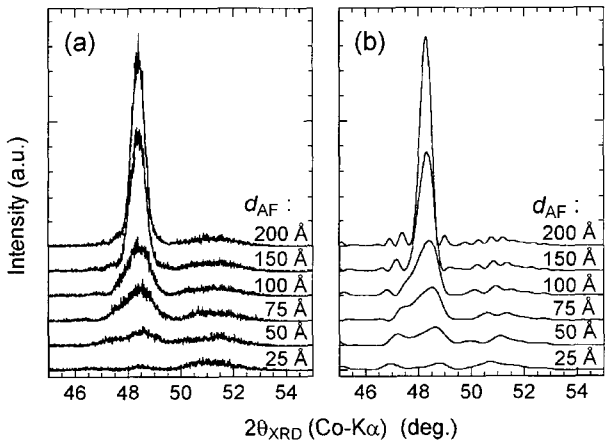

Fig. 2. Graphs (a) and (b) show measured and calculated X-ray diffraction profiles for polycrystalline Ni-Fe/$Mn_{74}Ir_{26}$ bilayer specimens. The individual curves are for different values of the antiferromagnetic layer thickness d_{AF}, as indicated. The "$2\theta_{XRD}$ (Co-Kα)" label on the horizontal axis refers to the scattering angle for the Cobalt Kα radiation.

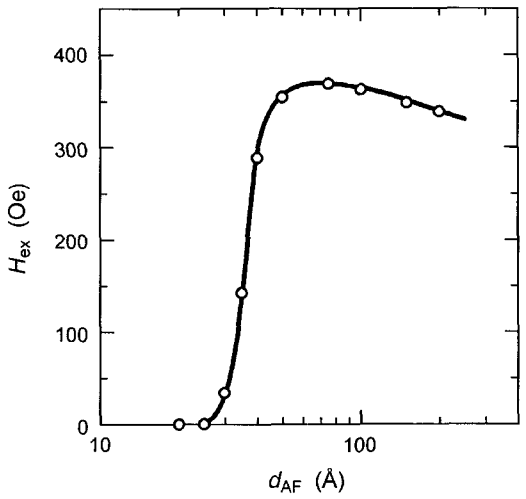

Fig. 4. The exchange biasing field H_{ex} as a function of the antiferromagnetic layer thickness d_{AF}, as obtained from the room temperature hysteresis loop measurements for polycrystalline Ni-Fe/$Mn_{74}Ir_{26}$ bilayers.

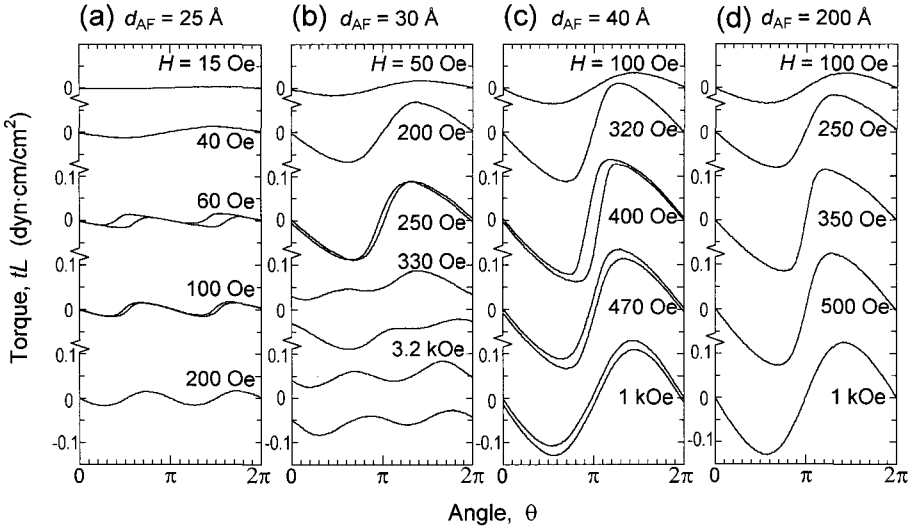

Fig. 5. Measured torque vs. field angle for polycrystalline Ni-Fe/$Mn_{74}Ir_{26}$ bilayers with a range of antiferromagnetic layer thickness d_{AF} values, as indicated for each panel, and for the indicated values of the applied in plane magnetic field H. The vertical axis shows the product of the torque per unit volume L and the film thickness t. The horizontal axis shows the in plane field angle θ relative to the field direction during the deposition.

the empirical $M_s d_F$ product value of 4.0×10^{-4} emu/cm^2, one obtains a unidirectional anisotropy constant $J_K \equiv M_s d_F H_{ex}$ of 0.147 erg/cm^2. From these hysteresis loop response, one can determine the critical thickness of the antiferromagnetic layer as $d_{AF}^{cr} = 37$ Å, at which H_{ex} takes half of its peak value.

Figure 5 shows the experimental torque response as a function of the applied in-plane field H and the AF layer thickness d_{AF} [14]. The vertical axes represent tL product, where L is the torque per unit volume and t is the total film thicknes, meaning the torque per unit film area. The horizontal axes give the in plane field angle relative to the deposition field direction. Panels (a) through (d) are for the indicated values of d_{AF}. The torque curves in each panel are for the indicated H values.

In the case of $d_{AF} = 25$ Å, the torque curve exhibits the sin θ character at low field ($H \leq 40$ Oe) which evolves into a sin 2θ characteristic at $H > 40$ Oe. The amplitude of the torque curves is always small. The rotational hysteresis loss tW_r, which was defined as the one-half the area enclosed between forward and reverse torque curves, also appears at the field higher than 40 Oe and decreases gradually and vanishes at high fields. When $d_{AF} = 30$ Å, the torque curve exhibits the sin θ characteristics in the low field ($H < 290$ Oe) and it changes to relatively flat response against the applied field direction, θ, with increasing field, while a small sin θ and sin 2θ components remain up to the high field. The rotational hysteresis loss is almost zero in the low field, appears at $H = 250$ Oe, and steeply increases at $H > 300$ Oe. With further increase of the field to 3.2 kOe, the rotational hysteresis loss remains almost constant.

As d_{AF} is increased above the critical antiferromagnetic layer thickness $d_{AF}^{cr} = 37$ Å, the torque response drastically changes. In the case of $d_{AF} = 40$ Å, the torque curve exhibits the sin θ characteristics under the whole field applied. The magnitude of the sin θ component gradually increases with increasing the field up to the critical field of 400 Oe, and saturates to be a value of 0.12 dyn·cm/cm^2. This value well corresponds to the unidirectional anisotropy constant of the same film $J_K = 0.11$ erg/cm^2, determined from the magnetization curve. Concerning the shape of torque curves in Fig. 5(c), a slope around $\theta = \pi$ gradually becomes large with increasing the field up to the critical field $H_{cr} = 400$ Oe. It gradually decreases with further increase of the field. The rotational hysteresis loss appears at $H \sim 400$ Oe and a small value of the rotational hysteresis loss still remains up to very high field. For the case of $d_{AF} = 200$ Å, the magnitude of the sin θ component gradually increases with increasing the field up to the critical field $H_{cr} \sim 400$ Oe, and slowly approaches to a saturated value of 0.13 dyn·cm/cm^2. The rotational hysteresis loss is not observed any more in the whole field range examined.

4. Single spin ensemble model

4.1. Modeling

From the microstructural analysis in the previous section, we found that the present Ni-Fe/Mn-Ir bilayers

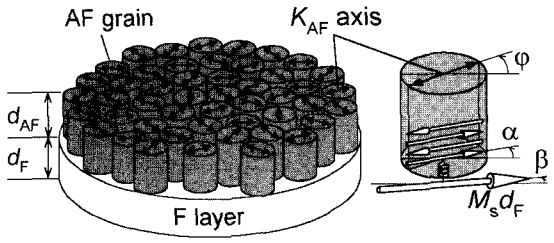

Fig. 6. A schematic model of the ferromagnetic (F)/antiferromagnetic (AF) bilayer ('single spin ensemble model'). The spin configuration in the F layer and in the AF grain, and the angular relations of them are indicated (right).

have polycrystalline structure and that the Mn-Ir grains have no preferred orientation in the film plane. By assuming the *magnetocrystalline anisotropy* of the AF grains as an origin of the magnetic anisotropy of the AF layer, we should take into account the random distribution of the anisotropy axes of the AF grains in the calculation model.

Figure 6 shows the schematic model of the F/AF bilayer [16, 17]. The ferromagnetic and antiferromagnetic layers have thicknesses d_F and d_{AF}, respectively. The F layer is regarded as a single domain (*i.e.*, the magnetization of the F layer is treated as a single spin). The AF layer is regarded as an aggregation of the AF grains whose magnetic anisotropy has uniaxial symmetry. The anisotropy axes of the AF grains lay in the film plane with 2-dimensonally random distributions. Here, we assume that the intergranular magnetic coupling of the AF grains is neglected and that the MB model is applicable between the F layer and the each AF grain. The MB model is shown schematically in the right-hand side of Fig. 6. The orientation angles for the ferromagnetic film magnetization vector and the antiferromagnetic spin axis are shown as β and α. The angle φ is the direction of the anisotropy axis of the AF grain, which is defined in the range from $-\pi/2$ to $\pi/2$. The small spring indicates the interface exchange coupling, J. No magnetic anisotropy has been taken into account for the ferromagnetic layer in this model. The in-plane magnetic field H is applied along the direction θ. The free energy of an AF grain per unit surface area, tE_{AF}, is given in the form:

$$tE_{AF} = K_{AF}d_{AF}\sin^2(\alpha-\varphi) - J\cos(\alpha-\beta). \quad (1)$$

In Eq. (1), K_{AF} is the uniaxial anisotropy constant in units of energy per unit volume for the antiferromagnetic grain, and J is the exchange coupling energy per unit area of the interface between the layers. From the partial derivation of Eq. (1) with α, one obtains the energy minimum equations, which determines the angle a under certain values of β and φ. Figure 7 shows contour maps of the

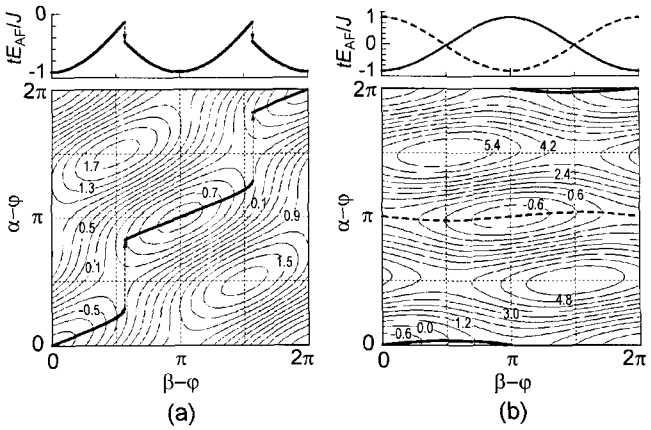

Fig. 7. Contour maps of the energy of AF grain as functions of deviation angles $\alpha-\varphi$ and $\beta-\varphi$, calculated for the cases of (a) $K_{AF}d_{AF}/J = 0.8$ and (b) $K_{AF}d_{AF}/J = 5$. The contour lines indicate the reduced energy, tE_{AF}/J. The upper part of respective map shows the changes of tE_{AF}/J along the thick lines in the contour map.

AF grain's energy as functions of deviation angles $\alpha-\varphi$ and $\beta-\varphi$, calculated with Eq. (1) for the cases of (a) $K_{AF}d_{AF}/J = 0.8$ and (b) $K_{AF}d_{AF}/J = 5$ [16, 17]. The reduced energy, tE_{AF}/J, is indicated by contour lines. The thick solid lines and the dashed one in the map indicate the loci of the angle $\alpha-\varphi$ which satisfying the energy minimum equations, when the angle $\beta-\varphi$ continuously changes from 0 to 2π (clockwise rotation). The changes of the reduced energy, tE_{AF}/J, along the loci are also indicated in the upper part of Fig. 7, as a function of the angle $\beta-\varphi$. In Fig. 7(a), when the direction of the F layer magnetization $\beta-\varphi = 0$, the direction of the AF spin axis $\alpha-\varphi = 0$. With increasing $\beta-\varphi$ up to 0.57π, $\alpha-\varphi$ follows behind $\beta-\varphi$ and becomes 0.28π. At the same time, tE_{AF}/J increases from -1 to -0.14. Then $\alpha-\varphi$ discontinuously jumps to the new angle 0.82π, and the energy portion of the AF grain is released irreversibly (dashed arrows in the figure). With further increasing $\beta-\varphi$ to π, $\alpha-\varphi$ precedes $\beta-\varphi$ and gradually increases to π. In the region, $\pi \le \beta-\varphi \le 2\pi$, we can see a similar change of $\alpha-\varphi$ against increasing $\beta-\varphi$. This means that the AF grain exhibits two-fold symmetry in its magnetic potential energy for a round rotation of the F layer magnetization. On the other hand, in Fig. 7(b), both loci always remain near $\alpha-\varphi = 0$ and π. This means that the direction of the AF spins is adhered to the anisotropy axis of the AF grain when the F layer magnetization rotates round.

By using the reduced energy of an AF grain along the loci as a function of the angle $\beta-\varphi$, $tE_{AF}(\beta-\varphi)$, which are indicated in the upper part of Fig. 7, and the geometrical distribution function of the anisotropy axes of the AF grains, $w(\varphi)$, the summation of the AF grain's energy per

unit area of the film plane is given as a function of β:

$$tE_{AF}^{total}(\beta) = \int_{-\pi/2}^{\pi/2} tE_{AF}(\beta-\varphi)w(\varphi)d\varphi. \quad (2)$$

In the present study, $w(\varphi) = 1/\pi$ was used for the calculation, because of the two-dimensionally random distribution of the anisotropy axes of the AF grains. The total energy of the system per unit area is thus obtained as a function of the strength (H) and the direction (θ) of the external applied field,

$$tE^{total} = tE_{AF}^{total}(\beta) - M_s d_F H\cos(\theta-\beta). \quad (3)$$

In Eq. (3), M_s denotes the saturation magnetization per unit volume of the ferromagnetic layer. The direction of the F layer magnetization, β, is determined to minimize Eq. (3) for certain values of H and θ, and one can calculate the magnetization processes of the F/AF bilayer. The detailed calculation procedure is given in Refs. 16-17.

4.2. Exchange bias field and magnetic torque response

Figure 8 shows the variation in H_{ex} as a function of the thickness parameter $K_{AF}d_{AF}/J$ calculated with single spin ensemble model. The vertical axis shows the model H_{ex} fields in terms of the reduced field parameter $M_s d_F H/J$.

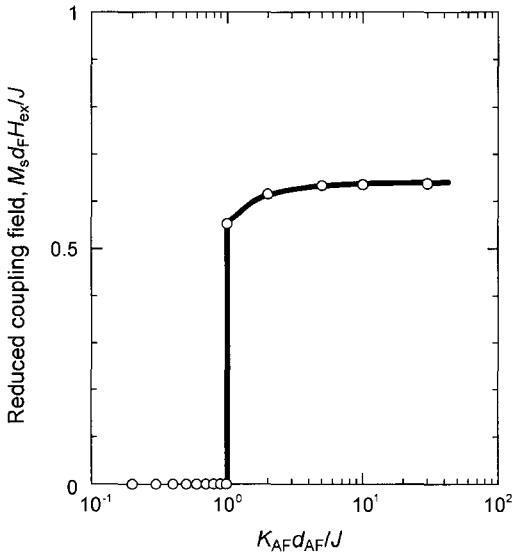

Fig. 8. The exchange biasing field H_{ex} as a function of the antiferromagnetic (AF) layer thickness d_{AF}, as obtained from the single spin ensemble model. The vertical field axis is given in terms of the reduced field parameter $M_s d_F H/J$, where M_s and d_F denote the magnetization and the thickness of the ferromagnetic layer, respectively, and J is the interface exchange coupling parameter. The horizontal thickness axis is given in terms of the reduced thickness parameter $K_{AF}d_{AF}/J$, where K_{AF} is the uniaxial anisotropy energy density for the AF layer.

These results show that the sudden appearance of H_{ex} occurs at a critical thickness value for d_{AF}. Comparing these calculated results with the experimental ones in Fig. 4, one can safely say that they qualitatively agree with each other. The critical thickness d_{AF}^{cr}, which may defined by $K_{AF}d_{AF}^{cr}/J = 1$ in the calculation, thus corresponds with the experimentally determined one in the previous section.

Figure 9 shows four panels of five calculated torque curves each. The vertical axes correspond to the tL product divided by the interfacial coupling energy J. The four panels, (a)~(d), reflect the effect of a systematic change in the $K_{AF}d_{AF}/J$ thickness parameter here, as shown. The graphs in each panel are for systematic changes in the $M_s d_F H/J$ field parameter, as indicated. First consider panel (a) for $K_{AF}d_{AF}/J < 0.5$. In this limit, d_{AF} is well below the d_{AF}^{cr} value introduced above. The graphs in (a) show that in this limit, the torque curve exhibits a completely flat response to the field direction and no hysteresis loss is observed, under any external applied field. When $K_{AF}d_{AF}/J$ exceeds 0.5, the situation changes. In the case of $K_{AF}d_{AF}/J = 0.8$, shown in panel (b), the torque curve exhibits a basic unidirectional sin q character at low field ($M_s d_F H/J = 0.02$) and the amplitude of it becomes large with increasing the applied field. When the applied filed parameter $M_s d_F H/J$ exceeds 0.118, the torque curve suddenly changes to the flat response to the field angle θ, and a rotational hysteresis loss appears simultaneously. The rotational hysteresis loss remains constant in higher field. When d_{AF} exceeds the critical thickness d_{AF}^{cr} and $K_{AF}d_{AF}/J$ exceeds unity, as in (c) and (d), the evolution in the torque character with field changes drastically. All of the torque curves show a sin θ character up to the highest fields. Here, moreover, no rotational hysteresis appears for any field.

Comparing the calculated torque results with the experimental ones shown in Fig. 5, one says that the single spin ensemble model elucidates the experimental magnetic torque results qualitatively.

4.3. Mechanism of direction control of the exchange anisotropy

In this section, the newly introduced single spin ensemble model is examined to elucidate a mechanism of the reversible inducement of the exchange anisotropy by field cooling procedure.

First, we describe the experimental fact [18, 19]. A polycrystalline Ni-Fe 50 Å/Mn-Ir 50 Å bilayer was first annealed at 300 °C for 0.5 hr to suppress the structural changes in the successive thermal annealing, then cooled to room temperature under an in-plane external applied field, $H_a = 1$ kOe along 0°-direction. The 0°-direction

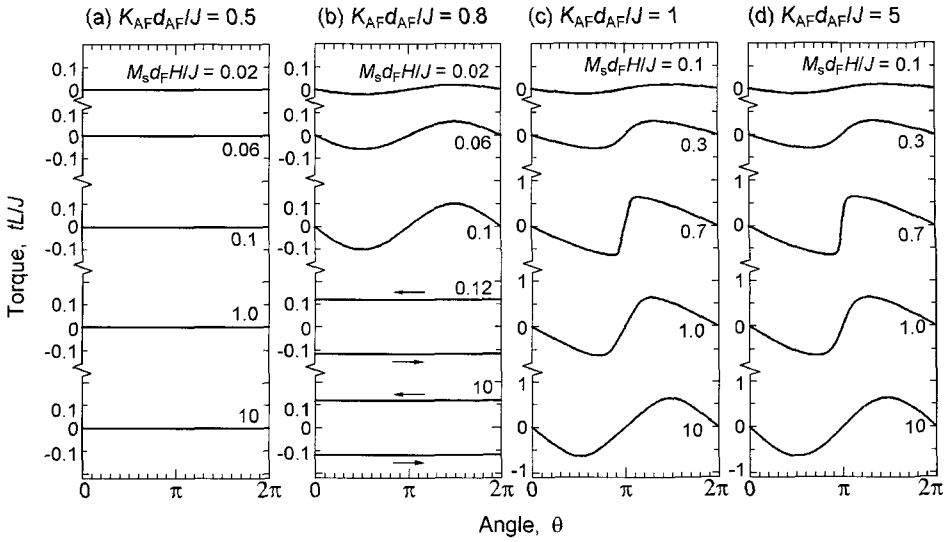

Fig. 9. Computed torque curves from the single spin ensemble model. The vertical axes show the torque per unit volume L in units of tL/J, where t is the bilayer thickness, and J is the interface exchange coupling parameter. The horizontal axes show the field angle θ. Panels (a) through (d) are for increasing values of the AF layer thickness d_{AF}, expressed in terms of $K_{AF}d_{AF}/J$, where K_{AF} is the uniaxial anisotropy energy density for the AF layer. The individual graphs in the panels are for different values of the in plane field H, expressed in terms of M_sd_FH/J, where M_s and d_F denote the magnetization and the thickness of the ferromagnetic layer, respectively.

coincided with the applied field direction during the deposition. The thickness of the AF layer, 50 Å, is thicker than the critical thickness, 37 Å, of the present bilayer system, as mentioned above. The blocking temperature of the specimen was 220 °C, beyond which the exchange anisotropy vanishes. The specimen was then annealed at 280 °C for 1 hr, and cooled to room temperature under H_a = 1 kOe. This procedure was performed three times in succession on the same specimen, changing the H_a direction as 90°, 0°, and 120°.

Figure 10 shows the changes of the *MH*-loops along respective two directions, measured with VSM, after each annealing procedure [19]. The specimen after the first annealing (a) shows the exchange anisotropy along 0°-direction, which agrees with the filed cooling direction. The exchange biasing field, H_{ex}, observed is 340 Oe. On the other hand, the *MH*-loop measured along 90°-direction is almost non-hysteresis and is characterized an S-shaped figure, of which magnetization is hard to be saturated. After the second and after annealing, the specimen shows the exchange anisotropy induced along the respective field cooling directions and shows a nearly constant biasing field of about 350 Oe. The corresponding experimental results were observed in the magnetic torque measurement [18]. The torque responses as a function of the applied field did not change at all for every specimen in each field cooling steps, except for the phase shift of the torque curves against the field direction θ, meaning

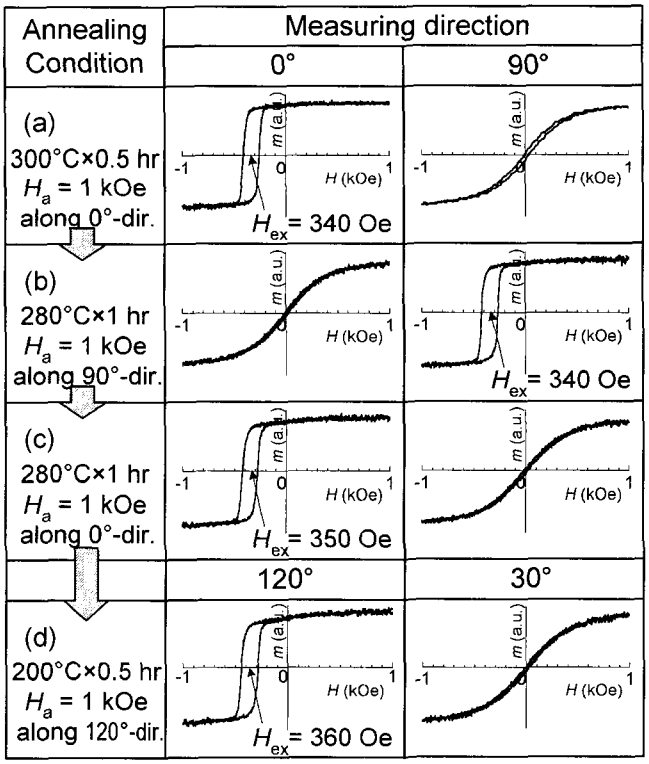

Fig. 10. Measured magnetization curves of Ni-Fe 50 Å/ $Mn_{74}Ir_{26}$ 50 Å polysrystalline bilayer after thermal annealing in a magnetic field of 1 kOe.

the change of the direction of the induced unidirectional anisotropy. These experimental result means the *reversible*

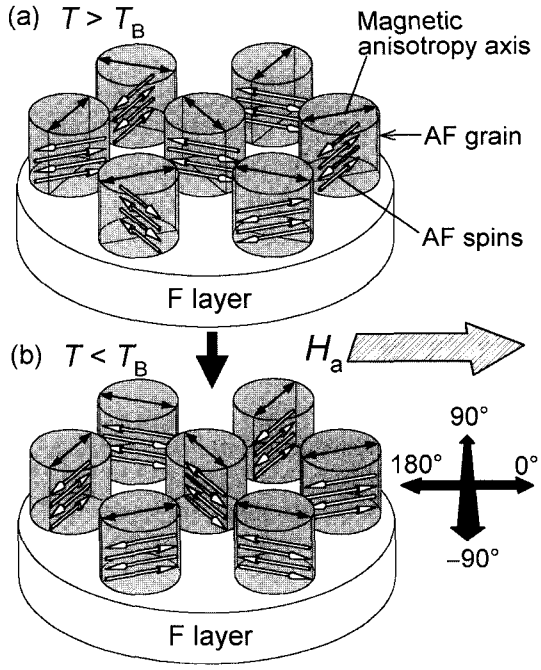

Fig. 11. Schematic view of the change of antiferromagnetic spin directions by field cooling in polycrystalline ferromagnetic/antiferromagnetic bilayer, based on the single spin ensemble model.

inducement of the exchange anisotropy of F/AF bilayer along the *desired direction* by field cooling.

Figure 11 illustrates a mechanism of the exchange anisotropy inducement by field cooling in polycrystalline bilayer, based on the single spin ensemble model [18, 19]. Two cases are shown for the temperature, T, (a) higher and (b) lower than the blocking temperature, T_B. The value of T_B is generally accepted as the temperature beyond which the thermal agitation energy exceeds the magnetic anisotropy energy to detach the direction of the AF spin axis from the anisotropy axis of the AF grains [20]. The spin axes of AF grains thus direct independently of the anisotropy axes of grains at $T > T_B$ (Fig. 11a). When the temperature becomes below T_B, the AF spin axes adhere to the anisotropy axes of the AF grains. At the moment, the external applied field, H_a, plays an important role through the saturation of the F layer magnetization. By assuming the ferromagnetic coupling, J, between the interfacial spins of both the F and the AF layers, the directions of spin axes of AF grains are selected to make the relative angle small between the interfacial spins. The directions of AF spin axes thus distribute from −90° to +90°, when H_a is applied along 0°-direction (Fig. 11b). When H_a is applied along 90°-direction, the directions of AF spin axes distribute from 0° to 180°, in a similar manner. Since this process brings about no structural

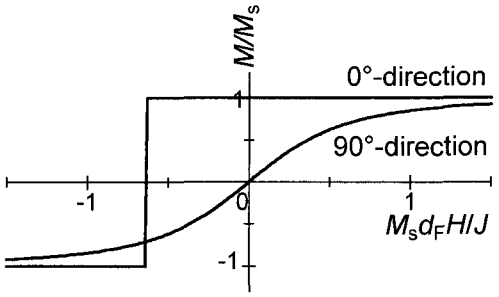

Fig. 12. Calculated magnetization curves with using single spin ensemble model. The antiferromagnetic spin directions at the interface are assumed to be distributed from −90° to +90°. Calculation parameter, $K_{AF} d_{AF}/J = 5$.

changes in the bilayers, it can completely occur reversibly.

Figure 12 shows the calculated MH-loops along 0°- and 90°-directions with the single spin ensemble model. The detailed calculation procedure is given in Ref. 16. The thickness parameter for the AF layer, $K_{AF} d_{AF}/J = 5$ was used for the calculation to illustrate the case of $d_{AF} > d_{AF}^{cr}$. The distribution of the directions of the AF spin axes, used for the calculation, was −90° to +90°. It is clearly seen that the exchange anisotropy is observed along 0°-direction and S-shaped loop is observed along 90°-direction. One finds a good agreement between this calculated result and the experimental data in Fig. 10, meaning the validity of the single spin ensemble model for the mechanism of the reversible inducement of the exchange anisotropy in polycrystalline bilayers by field cooling procedure.

5. Enhancement of exchange bias in Co-Fe (Ni-Fe)/Mn-Ir bilayers

Turn now to the experimental efforts to enlarge exchange anisotropy strength. We chose an Mn-Ir as the AF layer material in the present study, because it can derive relatively strong exchange anisotropy on the F layer with an ultra-thin thickness [21-24]. Effects of the chemical composition of both the F layer and the AF layer, the microstructure of the AF layer, and the interface between F and AF layers on the exchange bias in Co-Fe (Ni-Fe)/Mn-Ir bilayers are discussed in this section.

5.1. Effect of chemical composition of Mn-Ir

In the case of the so-called 'top type' Ni-Fe/Mn-Ir bilayers, in which the antiferromagnetic Mn-Ir layer is located on the ferromagnetic Ni-Fe layer, the Ir content and the sputtering conditions of Mn-Ir films strongly influence the exchange anisotropy. The present authors have reported that the unidirectional anisotropy constant

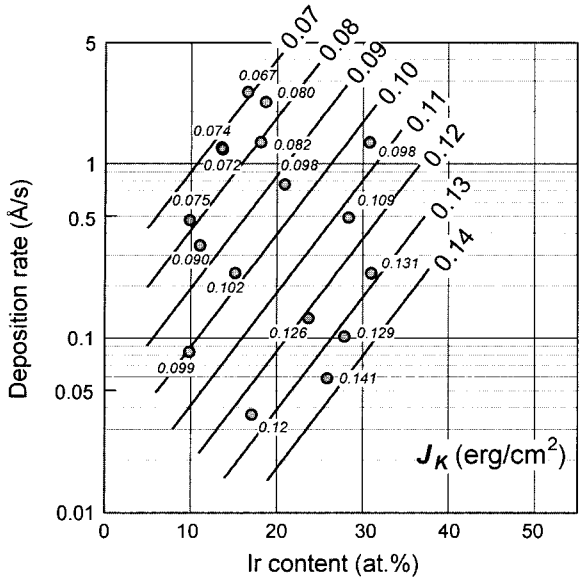

Fig. 13. A contour map of the unidirectional anisotropy constant, J_K, of as-deposited 'top type' Ni-Fe/Mn-Ir bilayers, as a function of Ir content and the deposition rate of the Mn-Ir films.

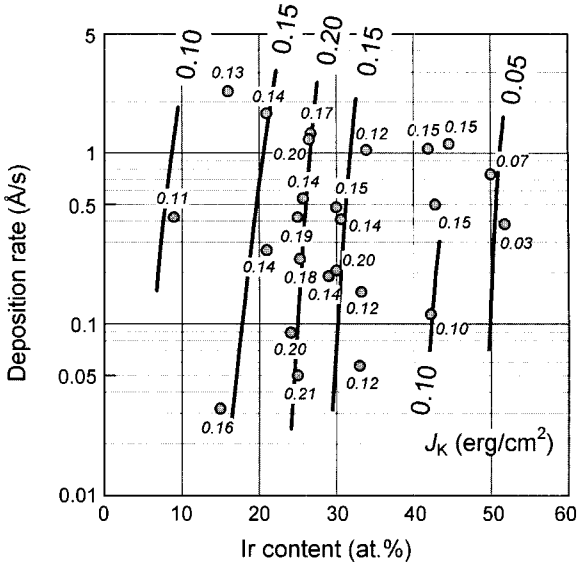

Fig. 14. A contour map of the unidirectional anisotropy constant, J_K, of 'bottom type' Mn-Ir/$Co_{90}Fe_{10}$ bilayers, annealed at 300 °C, as a function of Ir content and the deposition rate of the Mn-Ir films.

J_K monotonously increases with increasing the Ir content and decreasing the deposition rate of Mn-Ir films in as-deposited bilayers, as shown in Fig. 13, while the x-ray diffraction revealed no remarkable changes in the microstructure of Mn-Ir films corresponding to the variation in J_K [25]. This behavior of J_K, in particular, dependence on the deposition rate, was successfully explained by the single spin ensemble model, by taking into account the effective temperature of the films during deposition [15]. According to the above elucidation, the 'bottom type' bilayers, that are deposited under various sputtering conditions but annealed at *same* temperature (300 °C in the present study), should lose the dependence of J_K on the deposition rate. We thus investigated the exchange anisotropy of the 'bottom type' Mn-Ir/Co-Fe bilayer as a function of Ir content and the deposition rate of the Mn-Ir films.

Figure 14 shows a contour map of J_K as a function of the Ir content, x, in Mn-Ir layer and the deposition rate for the specimens, in the formed sub/underlayers/$Mn_{100-x}Ir_x$ 100 Å/$Co_{90}Fe_{10}$ 40 Å. Contours are aligned nearly vertical, meaning that J_K does not depend on the deposition rate. This behavior is quite deferent from that observed in the 'top type' Ni-Fe/Mn-Ir bilayers (Fig. 13) and is well exlained with the single spin ensemble model, as mentioned above. Concerning about the Ir content, J_K changes gradually. J_K, which is 0.1 erg/cm^2 around $x = 10$ at.%, increases with increasing x and reaches 0.2 erg/cm^2 at $x =$ 25 at.%. Beyond $x = 25$ at.%, J_K decreases and becomes less than 0.05 erg/cm^2 at $x = 50$ at.%. This compositional dependence of J_K well corresponds to the previous reports [26-28]. Hereafter, we choose the Ir content in Mn-Ir layer, x ~25 at.%.

5.2. Effect of microstructure of Mn-Ir layer

The microstructure of the antiferromagnetic layer is one of the most important factors to be controlled and it is easily influenced by various impurities during film deposition [29-31]. We thus fabricated $Ni_{79}Fe_{21}/Mn_{74}Ir_{26}$ bilayers, changing the purity of the sputtering atmosphere, and discussed the effect of impurities in the sputtering atmosphere on the microstructure and the respective magnetic properties of them. In the present study, in order to make two different purity of the sputtering atmosphere, the pressure of the sputtering chamber just before introducing ultra-clean Ar gas was prepared as less than 1×10^{-10} Torr in the extremely-clean (XC) process and as 3×10^{-7} Torr in the low-grade (LG) process, respectively [31, 32].

Figures 15 shows the changes of J_K as a function of the antiferromagnetic layer thickness, d_{AF} [32]. For the films fabricated in the LG process, J_K arises from 50 Å, reaches a peak around at $d_{AF} = 70$ Å, and then saturates about 0.05 erg/cm^2. On the other hand, for the films fabricated in the XC process, J_K arises from 30 Å, steeply increases to a value of 0.145 erg/cm^2 around at $d_{AF} = 50$ Å, and finally saturates about 0.14 erg/cm^2 in the region $d_{AF} >$ 100 Å. $J_K = 0.14$ erg/cm^2 is about three times larger than the saturated value of the LG processed films. The enhancement of J_K for the XC processed films is clearly

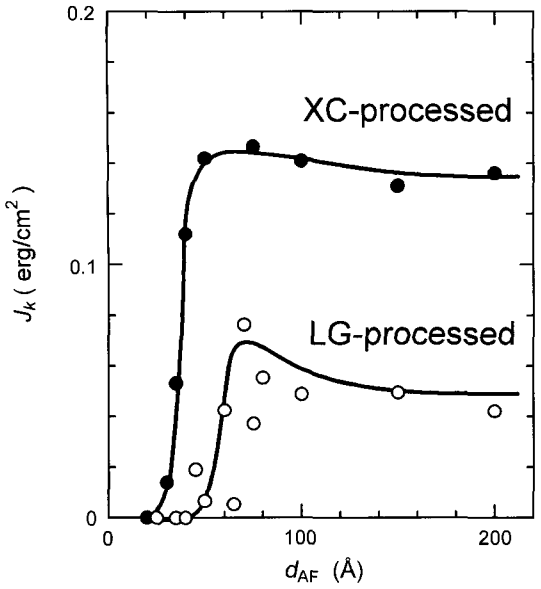

Fig. 15. The unidirectional anisotropy constant, J_K, of as-deposited Ni-Fe/$Mn_{74}Ir_{26}$ bilayers, as a function of the antiferromagnetic layer thickness, d_{AF}. Bilayers are fabricated under the extremely clean (XC) process and lower grade (LG) process, respectively.

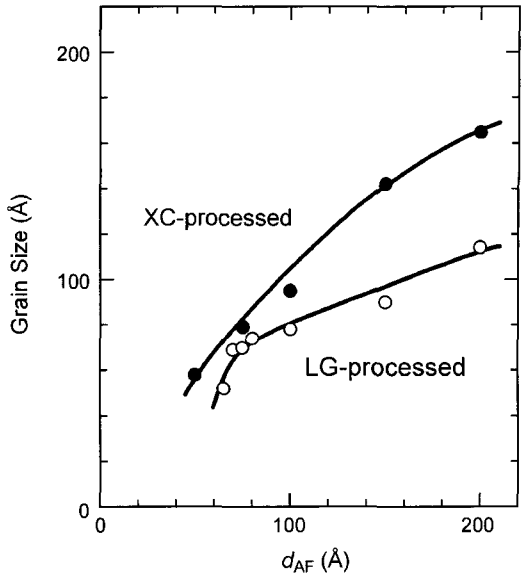

Fig. 16. The size of antiferromagnetic grains, determined from the Mn-Ir (111) diffraction line in the XRD profiles of Ni-Fe/$Mn_{74}Ir_{26}$ bilayers by using Scherrer's formula, as a function of the antiferromagnetic layer thickness, d_{AF}. Bilayers are fabricated under the extremely clean (XC) process and lower grade (LG) process, respectively.

correlated with the decrease of impurities in the films contaminated during the deposition process, because the fabrication conditions of both processed films were only differed in the pressure of the chambers before introducing sputtering Ar gas. The enhancement of J_K by decreasing the impurities in the sputtering atmosphere has been observed similarly in Ni-Fe/Mn-Ni bilayers [31].

Figure 16 shows the changes of the grain size of Mn-Ir, determined from the Mn-Ir (111) diffraction line in the XRD profiles of the specimens by using Scherrer's formula [33], as a function of d_{AF}. The AF grain size of the XC processed films is greater than that of the LG processed ones. When the AF grain size decreases, the thermal agitation of the AF spins becomes significant. Figure 17 shows the changes of J_K as a function of measuring temperature for the LG and the XC processed films, having d_{AF} = 100 Å [32]. During cooling or heating from R.T. to respective temperature, DC magnetic field of 1 kOe was applied parallel (circle symbol) or antiparallel (triangle symbol) to the direction of the unidirectional anisotropy induced in as-deposited films. At the respective temperature, a MH loop was measured and the J_K was determined. From the temperature dependence of J_K above R.T, it is found that J_K disappears at 420 K for the LG processed film, while J_K disappears at 560 K for the XC processed one. The temperature at which J_K disappears is a total blocking temperature of the film, T_B, and corresponds to the maximum of the distributed 'local blocking temperature', T_b [34-37]. The difference of J_K between the parallel (circle symbol) and the antiparallel (triangle symbol) directions on the field cooling at the respective measuring temperature, T (< R.T.), corresponds to the population of the AF grains, whose T_b are within

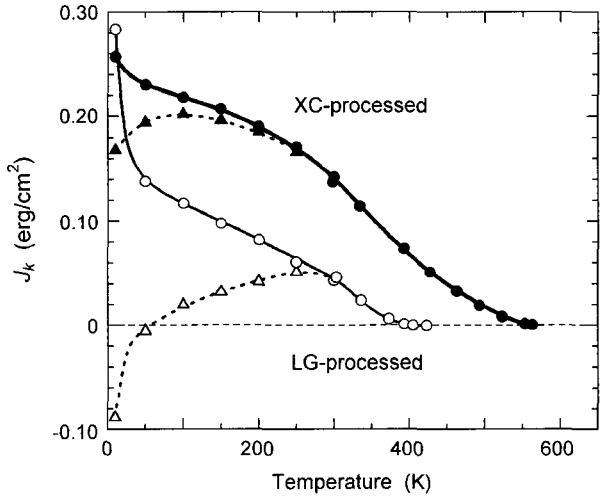

Fig. 17. Temperature dependence of the unidirectional anisotropy constant, J_K, of Ni-Fe/$Mn_{74}Ir_{26}$ bilayers as-deposited under the extremely clean (XC) process and lower grade (LG) process, respectively. Bilayers were cooled from room temperature to respective measuring temperature in a DC magnetic field of 1 kOe. Changes of J_K above room temperature in the heating process are also plotted.

the range between T and R.T [36]. As seen in Fig. 17, the difference of J_K between the parallel and the antiparallel cooling is clearly larger in the LG processed film, comparing with that in the XC processed one. Since spins in a small AF grain are easily flipped to the opposite direction by an agitation of thermal energy, T_b is mainly determined by the volume of the AF grain [20, 34, 35]. From these results, we conclude that the enhancement of J_K at R.T. for the XC processed films are originated from the enlargement of the volume of the AF grains.

5.3. Effect of interface modification by heat treatment of Mn-Ir surface

Since the exchange anisotropy is essentially derived from the magnetic coupling at the interface, the microstructure of the interface also should be controlled. The microstructure of the interface between the F and the AF layers has been generally controlled indirectly using the existing underlayers. In such a way, incidents other than the interface structure may influence simultaneously, and make it difficult to clarify the effect of the microstructural change of the interface on the exchange anisotropy. In the present study, in order to modify the interface (the surface of the Mn-Ir films of 'bottom type' bilayer) intentionally, specimens were heated after the deposition of Mn-Ir film under ultra high vacuum pressure [11]. In this section, we used specimens having a spin valve structure, in the formed, sub./Ta 50 Å/Ni-Fe 20 Å/$Mn_{74}Ir_{26}$ 68 Å/$Co_{90}Fe_{10}$ 20 Å/Cu 25 Å/$Co_{90}Fe_{10}$ 20 Å/Cu 10 Å/Ta 20 Å. The Ta/Ni-Fe bilayer placed under the Mn-Ir layer was used as an underlayer to promote fcc-(111) sheet texture of spin valves.

The specimens were heated by infrared (IR) irradiation from outside of the sputtering chamber through the sapphire (α-Al_2O_3) window. Pressure of the chamber was in the range of 10^{-11} Torr before the heat treatment in order to prevent the surfaces of the Mn-Ir films from contamination due to impurity gasses. Temperature of specimens (Ta/Ni-Fe/Mn-Ir films on the wafer) was varied in the range of 60 °C~230 °C, which was estimated from the temperature of the sample stage holding a wafer on it, by changing the current supplied to the IR lamp placed outside the chamber. Holding time at maximum temperature was 20 min~6 h. The specimens were then cooled to ~40 °C. After cooling down, a pinned layer (Co-Fe) and remaining layers were further deposited. An influence of the heat treatment on H_{ex} and T_B was investigated ex-situ.

Figure 18 shows the changes of J_K as a function of the holding time of heat treatment under the respective substrate temperature. H_{ex}, which was 0.8 kOe without heat

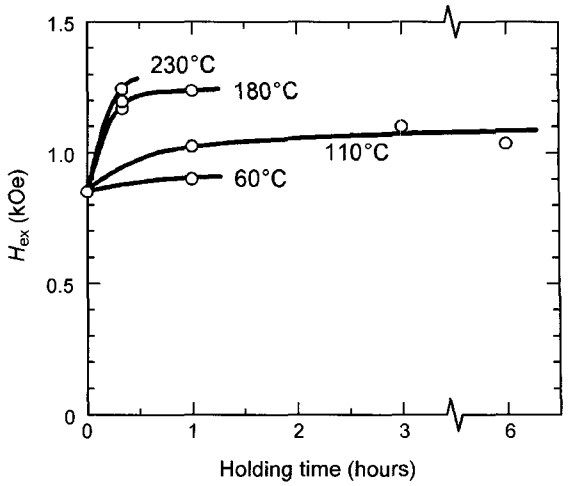

Fig. 18. The exchange biasing field H_{ex} as a function of the holding time of the *in-situ* heat treatment, as obtained from the room temperature hysteresis loop measurements for 'bottom type' $Mn_{74}Ir_{26}/Co_{90}Fe_{10}$ bilayers system in spin valves. After the deposition of Mn-Ir layer, the specimens were heated in ultra high vacuum by infrared irradiation up to the respective temperature. After cooling down the specimens to ~40 °C, a Co-Fe layer was deposited.

treatment, is enhanced up to 1.0 kOe using the heat treatment at 110 °C in 1 h. Furthermore, H_{ex} was enhanced up to 1.2 kOe using the heat treatment at 180 °C in 20 min. There were no remarkable changes in saturation magnetization of pinned Co-Fe layer. The value of H_{ex} = 1.2 kOe corresponds to 0.36 erg/cm^2 in J_K. Figure 19 shows the dependence of H_{ex} of the specimens on measuring temperature for both the specimen treated at 180 °C in 20 min and the specimen without heat treatment as a reference [11]. T_B clearly enhances from ~290 °C to ~325 °C after the in-situ heat treatment. In Fig. 20, representing the change of T_B as a function of the Mn-Ir layer thickness, one can recognize that T_B (~325 °C) of the specimen with d_{AF} = 68 Å, treated at 180 °C in 20 min, is comparable to that of the specimen fabricated under the conventional XC process (without heat treatment) with d_{AF} = 150 Å. It means that the *in-situ* heat treatment of the Mn-Ir surface is effective to realize ultra-thin spin valves having strong exchange anisotropy with excellent thermal stability.

In order to clarify the mechanism of enhancement of H_{ex} and T_B using the *in-situ* heat treatment, a microstructural analysis was carried out with XRD and X-ray reflectivity. However, remarkable differences within the accuracy of the experiment were not observed, meaning that no significant changes occurred in the interfacial roughness and the thickness of the Mn-Ir film. In addition, from the in-plane XRD measurement, which was

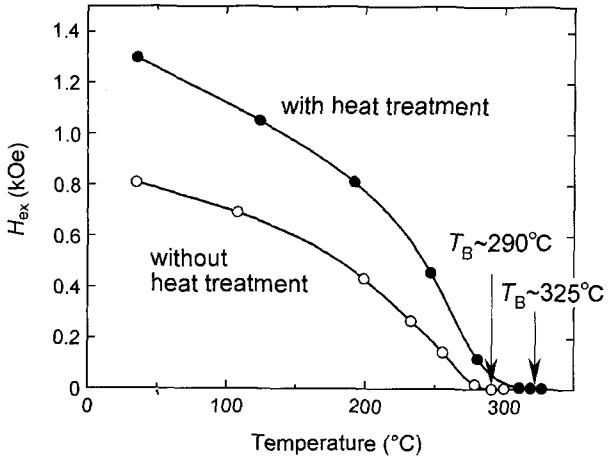

Fig. 19. Temperature dependence of the exchange biasing field H_{ex} of 'bottom type' $Mn_{74}Ir_{25}/Co_{90}Fe_{10}$ bilayers system in spin valves with and without the in-situ heat treatment (180 °C in 20 min) of the Mn-Ir surface. A Co-Fe layer was deposited after cooling down the specimens.

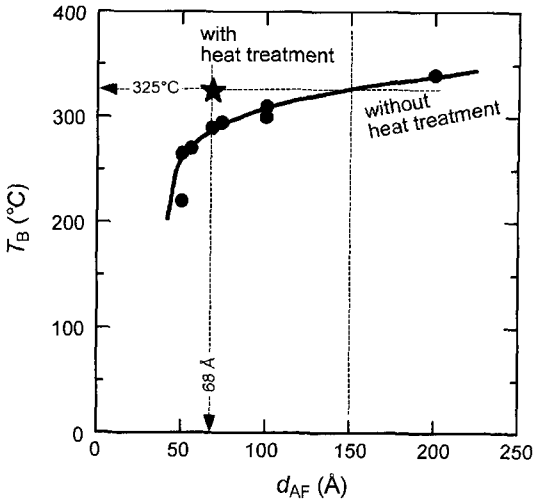

Fig. 20. The blocking temperature, T_B, of 'bottom type' $Mn_{74}Ir_{26}/Co_{90}Fe_{10}$ bilayers system with and without the in-situ heat treatment (180 °C in 20 min) of the Mn-Ir surface, as a function of the antiferromagnetic layer thickness, d_{AF}. A Co-Fe layer was deposited after cooling down the specimens.

carried out to examine the formation of ordered phase in Mn-Ir films, known as Mn_3Ir, only a fundamental diffraction from Mn-Ir (220) and no expected super lattice diffraction from Mn-Ir (110) was detected. As a whole, we say that some structural changes in the very surface of a Mn-Ir film, undetectable with XRD, occurred by heating a Mn-Ir film in vacuum, and resulted in the enhancement of H_{ex} and T_B. As for the reasons of the surface changes, atoms in the very surface of a Mn-Ir film may evaporate when heated in high vacuum pressure, and thus the surface composition or the surface morphology of a Mn-Ir film may be mainly changed.

5.4. Effect of chemical composition of Co-Fe

As mentioned earlier, the exchange coupling energy between the F and the AF layers (J), is one of the most important factors to derive large J_K values. Assuming Heisenberg exchange across the atomically smooth F/AF interface with the ferromagnetically aligned AF spins at the interface, J corresponds to $J_{ex}S_F \cdot S_{AF}/a^2$, where J_{ex} is the interfacial exchange integral, a is the lattice constant, S_F and S_{AF} are the spins of the interfacial atoms in the F and the AF layer, respectively. It is therefore expected to derive large J_K in the bilayer system, when we use the F layer with large magnetic moment [38]. The Co-Fe system is suitable for the systematic study about this subject, because of the well-known change of the moment against the chemical composition. We thus investigated the compositional dependence of J_K in $Co_{100-y}Fe_y$/Mn-Ir bilayer system.

In the structural analysis of the bilayers with XRD, no remarkable changes are observed as a function of the chemical composition of the F layer. In particular, for the AF layer whose microstructure sensitively affects the exchange anisotropy, as mentioned in section 5.2, no changes are naturally observed, because the Mn-Ir layer was deposited for the specimens under the same condition before the deposition of the $Co_{100-y}Fe_y$ layer. We thus expect that the following changes of the exchange anisotropy are due to the magnetization of the F layer.

Figure 21 shows the change of J_K as a function of the Fe concentration in $Co_{100-y}Fe_y$, for the cases of $d_{AF} = 50$ Å, 75 Å, and 100 Å. Regardless of the d_{AF} value, J_K steeply increases from 0.18 erg/cm^2 at $y = 10$ at.% with increasing y, and makes a broad peak over 0.5 erg/cm^2 around at $y = 30$ at.%~40 at.%. The maximum value obtained is 0.52 erg/cm^2 at $y = 38$ at.% in the case of d_{AF} = 50 Å. This value is 25% greater and more, compared to the largest value, that has ever been reported in the F/AF bilayer systems, including the systems using ordered AF materials such as NiMn [39] and PtMn [40]. Taking into account the ultra-thin AF layer of the present system, one fairly says that the $Co_{100-y}Fe_y$/Mn-Ir bilayer ($y = 30$ at.%~40 at.%) is very suitable for the pinned layer of spin valve element in the high-density magnetic recording head application. With a further increase in y, J_K gradually decreases and becomes 0.15 erg/cm^2 at $y = 100$ at.%, the pure Fe case. Comparing the change of J_K in relation to y with the compositional dependence of saturation magnetization of bulk Co-Fe alloy [41], which is also shown in a dashed line in Fig. 21, one can find a large discrepancy between them. In particular, the opposite trends of the J_K

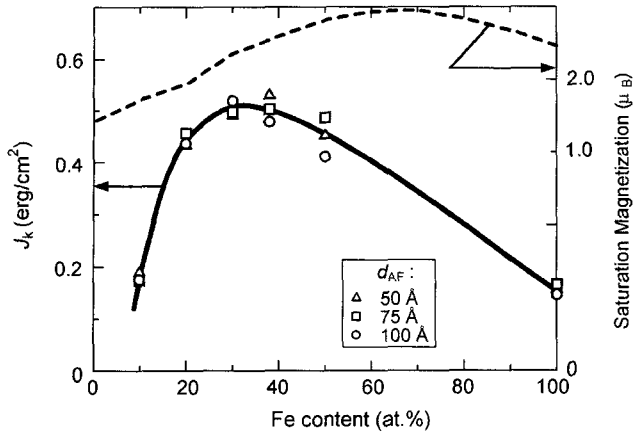

Fig. 21. Changes of the unidirectional anisotropy constant, J_K, of 'bottom type' $Mn_{75}Ir_{25}$/Co-Fe bilayers, annealed at 300 °C, as a function of the Fe concentration in Co-Fe layer. The antiferromagnetic layer thickness, d_{AF}, is 50, 75, and 100 Å, respectively.

and the saturation magnetization in relation to y are found in the 40 at.% $< y <$ 70 at.% region. If the Heisenberg expression for the interlayer exchange coupling energy (J) is available for the F/AF bilayer system, this experimental fact means that the magnetic moment of the interfacial atoms are different from that of the bulk alloys. One can imagine the electron transfer at the hetero-interface as an origin of the change of the magnetic moment at the interface; however, it requires further investigation.

The blocking temperature of the bilayer, T_B, is shown in Fig. 22 as a function of the Fe concentration in $Co_{100-y}Fe_y$, for the cases of d_{AF} = 50 Å, 100 Å, and 200 Å. Regardless of the d_{AF} value, there is no clear dependence of T_B on the Fe content. While T_B remains 220 °C even at d_{AF} = 50 Å, it reaches nearly 300 °C beyond d_{AF} = 100 Å. T_B = 300 °C

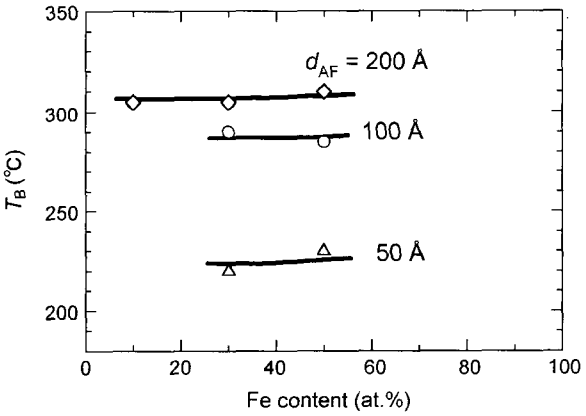

Fig. 22. The blocking temperature, T_B, of 'bottom type' $Mn_{75}Ir_{25}$/Co-Fe bilayers, annealed at 300 °C, as a function of the Fe concentration in Co-Fe layer. The antiferromagnetic layer thickness, d_{AF}, is 50, 100, and 200 Å, respectively.

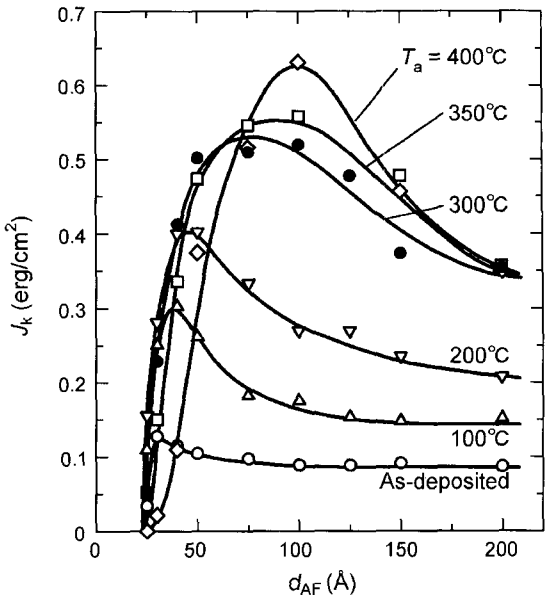

Fig. 23. The unidirectional anisotropy constant, J_K, of 'bottom type' $Mn_{75}Ir_{25}/Co_{70}Fe_{30}$ bilayers, annealed at various temperature, T_a, as a function of the antiferromagnetic layer thickness, d_{AF}.

is high enough for the application of the spin valve giant magnetoresistive devices.

Figure 23 shows the dependence of J_K on the AF layer thickness for the case of $Co_{70}Fe_{30}$, as a function of the annealing temperature, T_a. In as-deposited state, J_K shows relatively small value, regardless of d_{AF}. With increasing T_a, J_K gradually increases. Below T_a = 300 °C, the growing rate of J_K with increasing T_a is larger for the bilayers having thin d_{AF} than for those having thick d_{AF}. This behavior is consistent with the d_{AF} dependence of the blocking temperature, shown in Fig. 22. When T_a = 300 °C, J_K shows a broad peak over 0.5 erg/cm^2 around at d_{AF} = 50 Å~120 Å. From the application point of view, the broad peak of J_K against d_{AF} is favorable for the thickness control to obtain a large J_K value. The critical thickness of the AF layer, where J_K becomes half of the maximum value, is about 30 Å for the case of T_a = 300 °C. With further increasing T_a above 300 °C, J_K still increases in the bilayer with d_{AF} = 100 Å, while that in the bilayer with $d_{AF} <$ 70 Å remarkably decreases. It means that the exchange anisotropy of $Co_{70}Fe_{30}$/Mn-Ir 100 Å bilayer is stable for thermal annealing up to 400 °C. It is sufficiently high for the application of the spin valve tunnel magnetoresistive devices in the magnetic random access memories.

7. Summary

The role of magnetic anisotropy of the antiferromagnetic layer on the magnetization process of exchange coupled

polycrystalline ferromagnetic/antiferromagnetic bilayers is discussed. In order to elucidate the magnetic torque response of Ni-Fe/Mn-Ir bilayers, the single spin ensemble model is newly introduced, taking into account the two-dimensionally random distribution of the magnetic anisotropy axes of the antiferromagnetic grains. The mechanism of the reversible inducement of the exchange anisotropy along desirable directions by field cooling procedure is successfully explained with the new model. Unidirectional anisotropy constant, J_K, of polycrystalline Ni-Fe/Mn-Ir and Co-Fe/Mn-Ir bilayers is investigated as functions of the chemical composition of both the ferromagnetic layer and the antiferromagnetic layer. The effects of microstructure and surface modification of the antiferromagnetic layer on J_K are also discussed. As a notable result, an extra large value of J_K, which exceeds 0.5 erg/cm^2, is obtained for $Co_{70}Fe_{30}$/$Mn_{75}Ir_{25}$ bilayer with the ultra-thin (50 Å~100 Å) Mn-Ir layer. The exchange anisotropy of $Co_{70}Fe_{30}$ 40 Å/$Mn_{75}Ir_{25}$ 100 Å bilayer is stable for thermal annealing up to 400 °C, which is sufficiently high for the application of spin valve magnetoresistive devices.

References

[1] See, e.g., J. Nogués and I. K. Schuller, J. Magn. Magn. Mater. **192**, 203 (1999).

[2] W. H. Meiklejohn and C. P. Bean, Phys. Rev. **102**, 1413 (1956); **105**, 904 (1957).

[3] W. H. Meiklejohn, J. Appl. Phys. **33**, 1328 (1962).

[4] D. Mauri, H. C. Siegmann, P. S. Bagus, and E. Kay, J. Appl. Phys. **62**, 3047 (1987).

[5] M. D. Stiles and R. D. McMichael, Phys. Rev. B **59**, 3722 (1999).

[6] H. Xi and R. M. White, Phys. Rev. B **61**, 80 (2000).

[7] V. S. Speriosu, B. A. Gurney, D. R. Wilhoit, and L. B. Brown, *Digests of the INTERMAGi96 Coference*, Seattle, Washington, 1996.

[8] H. Berg, W. Clemens, G. Gieres, G. Rupp, W. Schelter, and M. Vieth, IEEE Trans. Magn. **32**, 4624 (1996).

[9] K. Okuyama, T. Shimatsu, S. Kuji, and M. Takahashi, IEEE Trans. Magn. **31**, 3838 (1995).

[10] M. Takahashi, M. Tsunoda, and H. Shoji, Vacuum **59**, 814 (2000).

[11] K. Yagami, M. Tsunoda, and M. Takahashi, J. Appl. Phys. **89**, 6609 (2001).

[12] A. Segmuller and A. E. Blackeslee, J. Appl. Cryst. **6**, 19 (1973).

[13] I. K. Schuller, Phys. Rev. Lett. **44**, 1597 (1980).

[14] M. Tsunoda, Y. Tsuchiya, T. Hashimoto, and M. Takahashi, J. Appl. Phys. **87**, 4375 (2000).

[15] K. Yagami, M. Tsunoda, and M. Takahashi, J. Appl. Phys. **87**, 4930 (2000).

[16] M. Tsunoda and M. Takahashi, J. Appl. Phys. **87**, 4957 (2000).

[17] M. Tsunoda and M. Takahashi, J. Appl. Phys. **87**, 6415 (2000).

[18] M. Tsunoda, T. Hashimoto, M. Konoto, and M. Takahashi, J. Magn. Soc. Jpn. **25**, 827 (2001).

[19] M. Tsunoda and M. Takahashi, J. Magn. Magn. Mater. **239**, 149 (2002).

[20] E. Fulcomer and S. H. Charap, J. Appl. Phys. **43**, 4190 (1972).

[21] M. Mao, S. Funada, C.-Y. Hung, T. Schneider, M. Miller, H.-C. Tong, C. Qian, and L. Miloslavsky, IEEE Trans. Magn. **35**, 3913 (1999).

[22] J. Driel, R. Coehoorn, K.-M. H. Lenssen, A. E. T. Kuiper, and F. R. Boer, J. Appl. Phys. **85**, 5522 (1999).

[23] M. Pakala, Y. Huai, G. Anderson, and L. Miloslavsky, J. Appl. Phys. **87**, 6653 (2000).

[24] G. Anderson, Y. Huai, and L. Miloslavsky, J. Appl. Phys. **87**, 6989 (2000).

[25] K. Yagami, M. Tsunoda, S. Sugano, and M. Takahashi, IEEE Trans. Magn. **35**, 3919 (1999); ibid. **36**, 612 (2000), as an erratum.

[26] K. Hoshino, R. Nakatani, H. Hoshiya, Y. Sugita, and S. Tsunashima, Jpn. J. Appl. Phys. **35**, 607 (1996).

[27] H. N. Fuke, K. Saito, Y. Kamiguchi, H. Iwasaki, and M. Sahashi, J. Appl. Phys. **81**, 4004 (1997).

[28] A. J. Devasahayam, P. J. Sides, and M. H. Kryder, J. Appl. Phys. **83**, 7216 (1998).

[29] K. Uneyama, M. Tsunoda, and M. Takahashi, IEEE Trans. Magn. **33**, 3685 (1997).

[30] M. Tsunoda, M. Konoto, K. Uneyama, and M. Takahashi, IEEE Trans. Magn. **33**, 3688 (1997).

[31] M. Tsunoda, K. Uneyama, T. Suzuki, K. Yagami, and M. Takahashi, J. Appl. Phys. **85**, 4919 (1999).

[32] M. Takahashi, M. Tsunoda, and K. Uneyama, J. Magn. Magn. Mat. **209**, 65 (2000).

[33] B. D. Cullity, *Element of X-ray diffraction (2nd edition)*, Addison-Wesley, Reading, MA, 1978, p. 102.

[34] K. Nishioka, C. Hou, H. Fujiwara, and R. D. Metzger, J. Appl. Phys. **80**, 4528 (1996).

[35] K. Nishioka, S. Shigematsu, T. Imagawa, and S. Narishige, J. Appl. Phys. **83**, 3233 (1998).

[36] M. Tsunoda, Y. Tsuchiya, M. Konoto, and M. Takahashi, J. Magn. Magn. Mat. **171**, 29 (1997).

[37] S. Soeya, T. Imagawa, K. Mitsuoka, and S. Narishige, J. Appl. Phys. **76**, 5356 (1994).

[38] F. T. Parker, K. Takano, A. E. Berkowitz, Phys. Rev. B **61**, R866 (2000).

[39] T. Lin, C. Tsang, R. E. Fontana, and J. K. Howard, IEEE Trans. Magn. **31**, 2585 (1995).

[40] M. Saito, Y. Kakihara, T. Watanabe, and N. Hasegawa, J. Magn. Soc. Jpn. **21**, 505 (1997).

[41] R. M. Bozorth, *Ferromagnetism*, IEEE Press, New York, 1993, p. 195.